Energy transfer processes involving different luminescence centres in BaF_2:Ce

1993 J. Phys.: Condens. Matter 5 1659

(http://iopscience.iop.org/0953-8984/5/11/007)

J. Phys.: Condens. Matter 5 (1993) 1659–1680. Printed in the UK

Energy transfer processes involving different luminescence centres in BaF_2:Ce

R Visser†, P Dorenbos†, C W E van Eijk†, A Meijerink‡, G Blasse‡ and H W den Hartog§

† Radiation Technology Group, Department of Applied Physics Delft University of Technology, Mekelweg 15, 2629 JB Delft, The Netherlands

‡ Debye Research Institute, University of Utrecht, PO Box 80000, 3508 TA Utrecht, The Netherlands

§ Solid State Physics Laboratory, State University of Groningen Nijenborgh 18, 9747 AG Groningen, The Netherlands

Received 18 August 1992, in final form 4 December 1992

Abstract. *The luminescence of cerium-doped barium fluoride crystals has been* investigated as a function of wavelength and time. For excitation UV light, x-rays and gamma rays were used. The well known cross luminescence (CL) near 200 nm and self-trapped exciton luminescence (STE) near 300 nm, which are due to excitations of the host lattice, are observed at low cerium concentrations. For increasing cerium concentrations, the CL and STE emission is gradually replaced with cerium emission. Luminescence due to at least three different cerium related centres was found.

The decay of the luminescence under gamma excitation is non-exponential. At low cerium concentrations, its duration is much longer than the decay time of the excited level of the predominant cerium centre. At higher cerium concentrations, the luminescence decays faster.

These observations are explained in terms of an energy transfer model. The cerium luminescence due to energy transfer from CL and STE centres was calculated using the parameters obtained from experiment. Comparing the calculations to the observed photon outputs and decay curves leads to an interpretation of the luminescence mechanism in BaF_2:Ce. Apart from radiative and dipole–dipole energy transfer from CL and STE centres to cerium centres, transfer from the STE to unknown centres also plays a role, as well as direct excitation of cerium centres by free or trapped electrons and holes.

1. Introduction and model

BaF_2 is a well known scintillator, mainly because of its high density and its sub-nanosecond cross luminescence (CL) bands at 195 nm and 220 nm [1–5]. However, as well as this luminescence self-trapped exciton (STE) luminescence is observed near 300 nm having a decay time of about 630 ns [2, 6]. This relatively slow STE luminescence is not desired in many scintillator applications. Doping the BaF_2 crystal with Ce^{3+} causes the STE luminescence to disappear, as was shown by scintillation studies on crystals doped with 0–30 mol.% [7–12]. The Ce^{3+} ion is an attractive dopant because of its large radiative transition probability [13]. The cerium luminescence, which replaces the STE emission, has a shorter effective decay time than the STE. A disadvantage is that the CL also disappears by the doping. On the other hand, for detection of CL, photomultipliers with an (expensive) fused silica window are required,

0953-8984/93/111659+22$07.50

whereas for detection of the cerium luminescence (at longer wavelengths) an ordinary glass window is sufficient.

The above mentioned investigations did not yield detailed information concerning the luminescence decay of BaF_2:Ce after excitation by a gamma quantum. Only effective decay times were reported. Also, no distinction was made between luminescence contributions from different centres in the crystal. Since both are important for understanding the processes involved in the transformation of the gamma energy to luminescence, we performed the present study.

In earlier papers [11, 12, 14] we published the emission spectra and the luminescence decay of BaF_2:Ce under high-energy photon excitation, i.e. x-rays and gamma rays. The emission spectra show a rather complicated structure. Also, the luminescence decay cannot be described in a simple way. In this paper we offer an explanation for both observations.

The emission spectra of BaF_2:Ce show that high-energy photons give rise to different emission bands. First, there are the above-mentioned CL and STE bands. Also, due to the cerium doping, several cerium-related emission bands, in this paper denoted as Ce_1, Ce_2 and Ce_3, are observed. These bands will be discussed in section 3.1. For convenience of notation, we denote the centres related to the emission bands as CL, STE, Ce_1, Ce_2, and Ce_3 centres, respectively.

A schematic representation of the model adopted for explaining the luminescence from BaF_2:Ce is shown in figure 1. After the absorption of a high-energy photon in the crystal, hot free electrons and holes are created. By Auger processes and phonon emission, these will cool down within some tens of picoseconds, as was also observed in alkali halides [15]. The holes can become self-trapped, thus forming V_K centres. Holes may also be trapped at interstitial F^- ions, thus forming V_H centres. The electrons are less likely to be self-trapped. Instead, they can be trapped at fluorine vacancies, thereby forming F centres. Also, we expect that electrons may be trapped near Ce^{3+} ions, yielding the centre denoted Ce-e in figure 1.

During the short period in which free hot electrons and holes exist, CL centres can be created. These centres consist of a hole in the $Ba(5p^6)$ band, which may be considered as localized near one Ba ion [16]. This centre decays radiatively at the moment an electron from the $F^-(2p^6)$ valence states recombines with the hole. Free electrons and holes may also come together to form a free exciton, which gets self-trapped at a later stage, yielding an STE. If free electrons and holes recombine near a Ce^{3+} centre, this centre may be excited (excited cerium centres are denoted by Ce^* in figure 1).

After the electrons and holes are (self-) trapped, the following processes may occur. Trapped holes can diffuse through the crystal [17]. Depending on the trapping mechanism, the electron is also more or less mobile. If trapped electrons and holes meet, an STE may be formed.

So far, we have considered the direct excitation processes shown in figure 1. We can also have energy transfer from the directly excited centres to cerium centres. The CL and STE centres can transfer their energy non-radiatively to the cerium centres, provided that the CL and STE emission spectra overlap the cerium absorption spectra. Then photons, emitted by CL and STE centres, can also excite the cerium centres (radiative energy transfer). Finally, once cerium centres are excited, energy transfer to other cerium centres plays a role. Since the decay of the CL, STE, and excited cerium centres are all dipole-allowed, non-radiative energy transfer between these centres will proceed through the dipole–dipole interaction mechanism [18–20].

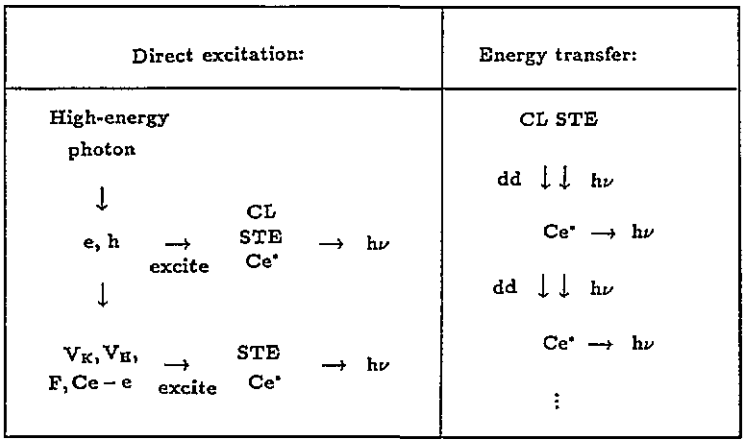

Figure 1. Schematic of the centres and processes used in the model. dd = transfer through dipole–dipole interaction; $h\nu$ = (emitted) photon.

To summarize, we distinguish four main contributions to the luminescence: (i) prompt luminescence due to emission by centres excited within the first few picoseconds by hot holes and electrons, (ii) delayed luminescence due to excitation of centres by (self-) trapped charge carriers, (iii) luminescence due to dipole–dipole energy transfer, and (iv) luminescence due to absorption of photons emitted from other centres in the crystal.

The contributions (iii) and (iv) can be calculated relatively straightforwardly if absorption and emission spectra and the decay times of the relevant centres are known. The absorption spectra and decay times were obtained in the 'preparatory measurements' presented in section 3.1. In section 3.2, the emission and decay data, obtained from BaF_2:Ce crystals irradiated with high-energy photons, are presented. In section 4.1 we present the method used for calculating contributions (iii) and (iv) to the luminescence observed in section 3.2. In sections 4.2 and 4.3 results from these calculations are compared to the experimental data.

2. Experimental techniques

The crystals investigated were grown using the Bridgman technique. The crystals were grown in a helium atmosphere, containing less than 0.1 ppm of O_2. As starting chemicals, BaF_2 powder (Merck 1725 optipure) and CeF_3 (99.9% pure Hicol/Johnson Matthey/Ventron 21118) were used. For each crystal, about 7 g of the chemicals were used, to which 0.1 g up to 0.4 g of PbF_2 (Merck 7387 suprapure) was added as an oxygen scavenger. After growth, the cylindrically shaped crystal boules, with a diameter of 7–8 mm, were cut perpendicular to the symmetry axis and polished at the top and bottom faces. The cerium concentrations were calculated from the weighted-in amounts of CeF_3. An exception to this is the 0.0012 mol.% doped sample, the concentration of which was determined from absorption spectra.

Optical absorption and emission spectra were measured using an ARC VM502 monochromator, an ARC 775 deuterium lamp and a Thorn EMI 9426 or a Philips XP2020Q photomultiplier tube. Excitation spectra were measured using a Spex

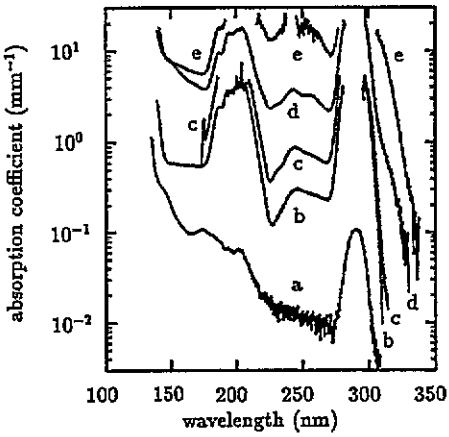

Figure 2. Optical absorption of BaF_2:Ce. The cerium contents (mol.%) are (a) 0.0012, (b) 0.17, (c) 0.38, (d) 0.83, (e) 2.6. The crystal thicknesses d (mm) are (a) 4.3, (b) 1.88, (c) 1.88, (d) 0.38, (e) 0.35. The wavelength resolution is 3 Å FWHM.

Fluorolog spectrofluorometer. Luminescence decay of the different cerium centres was measured using light from an Edinburgh flash lamp filled with deuterium. The pulse width was 6 ns FWHM (full width at half maximum). The light from this lamp was made monochromatic using interference filters. High-energy photon excitation of the crystals was performed with an x-ray tube with a copper anode and operated at 35 kV. The resulting luminescence was recorded as a function of wavelength. Luminescence decay was measured using a ^{137}Cs source, which emits 662 keV gamma quanta. This measurement is based on the single-photon counting technique described by Bollinger and Thomas [21], and had a time resolution of 0.5 ns FWHM. All experimentally obtained data were corrected using the calibration curves for the equipment. In the decay measurements, no correction was made for the wavelength dependence of the photomultiplier detection efficiency.

3. Results

In subsection 3.1, the preparatory measurements are discussed. In section 3.2, the luminescence due to irradiation of the crystals with x-rays or gamma rays is presented.

3.1. Preparatory measurements

3.1.1. Absorption. Figure 2 shows the absorption spectra of several cerium-doped BaF_2 crystals. The absorption coefficient was calculated as $\mu = -(1/d)\ln(T/T_{max})$, where d is the crystal thickness, T is the transmission, and T_{max} is the maximum transmission. The latter was about 0.93, and not 1, which is due to reflective losses at the air-to-crystal interfaces. In the region between 220–270 nm, one should not interpret curve a as giving the absorption coefficient of the bulk material. The main contribution here is related to surface absorption and to the wavelength dependence of the reflective losses. This was found by comparing crystals with different thicknesses. In the region between 300–700 nm, which is not shown in the figure, μd was less than 0.1 for all samples.

Absorption spectra similar to those in figure 2 were observed by Loh in Ce^{3+} doped CaF_2, SrF_2, and BaF_2 [22]. The absorption edge near 138 nm in figure 2, curve a, corresponds to $F^-(2p^6) \rightarrow Ba^{2+}(6s)$ charge transfer, which gives rise to STE formation [23]. Following the interpretation of Loh, the shift of this edge to longer wavelengths caused by cerium doping may be assigned to $F^-(2p^6) \rightarrow Ce^{3+}(6s)$ charge transfer. This would yield excitons associated with Ce^{3+} ions. The shoulder at 148 nm in figure 2, curves a and d, may be due to excitons associated with another impurity. This band was not observed in all samples.

The absorption bands at 200 nm and 290 nm can be assigned respectively to the split $5d(t_{2g})$ and $5d(e_g)$ levels of the Ce^{3+} ion at a cubic Ba^{2+} site. The splitting arises from spin–orbit coupling and the electric field caused by the neighbouring charge compensating F^- interstitial [24]. In BaF_2, this F^- ion is mainly located at a next-nearest neighbour interstitial site [25, 26]. Hence, the $Ce^{3+}_{Ba} - F^-_i$ centre has C_{3v} symmetry. Also, in an appreciable fraction of the centres, the F^- interstitial is located at a nearest-neighbour site, yielding C_{4v} symmetry. The absorption bands near 245 nm can be assigned to clusters of Ce^{3+} ions, in analogy with the CaF_2 case [22, 24]. Note that this absorption is much less pronounced in BaF_2 than it is in CaF_2 at the same cerium concentration. Less pronounced clustering in BaF_2, relative to CaF_2, was also found in audio-frequency capacitance measurements [25]. The absorption shoulder at 310 nm, which is most pronounced at the higher cerium concentrations, reminds one of the *A* band in CaF_2 [24], which is also located at longer wavelengths than the main Ce^{3+} $4f \rightarrow 5d(e_g)$ absorption. In analogy with Manthey's interpretation of this band in CaF_2, we may assign it tentatively to a $Ce^{3+}_{Ba} - O^{2-}_F$ centre, with the oxygen at a nearest-neighbour substitutional F^- site.

In CaF_2, beside the main Ce^{3+} $4f \rightarrow 5d(e_g)$ absorption band, many others were found at slightly different wavelengths [24]. Their intensity differed between different samples. This indicates that each absorption band contains contributions from many more-or-less similar cerium centres. This is to be expected in BaF_2, too. We could not distinguish between these centres. Therefore, we will denote all centres related to the 200 nm and 290 nm absorption bands as Ce_1. The centres related to the absorption near 310 nm will be denoted as Ce_2 and those related to the absorptions near 245 nm as Ce_3. If one assumes that the Ce_2 and Ce_3 absorption bands have a shape similar to that of the 290 nm absorption band, and that they are equally strong (i.e. the same oscillator strength), then one can estimate the concentration of the Ce_2 and Ce_3 centres. This is shown in table 1. We stress the fact that the data in table 1 are rough estimates. The estimated centre concentration may differ from the real value by a constant factor.

Table 1. Concentrations of the Ce_2 and Ce_3 centres in our samples estimated using absorption data and assuming that the oscillator strengths of these centres are the same as for Ce_1.

Cerium conc. (mol.%)	Ce_2 conc. (mol.%)	Ce_3 conc. (mol.%)
0.0012	$<4 \times 10^{-5}$	$<1 \times 10^{-4}$
0.17	$<2 \times 10^{-4}$	$(3.3 \pm 0.3) \times 10^{-3}$
0.38	$<2 \times 10^{-4}$	$(10 \pm 1) \times 10^{-3}$
0.83	$(7 \pm 2) \times 10^{-3}$	$(3.9 \pm 0.3) \times 10^{-2}$
2.6	0.12 ± 0.03	0.25 ± 0.05
4.9	0.18 ± 0.07	>0.05

Apart from the absorption discussed above, which is for non-irradiated samples, an additional broad absorption peaking at 510 nm emerges on x-irradiation of the crystals. This causes a pink colouration of these crystals, extending up to 0.2 mm below the crystal surface. This colouration was reported earlier [12]. Figure 3 shows this absorption in the 2.6 mol.% doped crystal after irradiation with x-rays for 800 s, which delivered a total energy of 4×10^{15} MeV per m^2 of crystal surface. In the 0.83 mol.% doped sample, this absorption was 0.27 times as strong as in the 2.6 mol.% doped sample after the same dose. After x-irradiation, we observed a similar absorption in lanthanum-doped BaF_2 [6]. In BaF_2 doped with 0.01 wt% of trivalent rare-earth impurities (except for Sm and Eu) a similar band was also observed by Vakhidov and co-workers [27] at 77 K after gamma-irradiation.

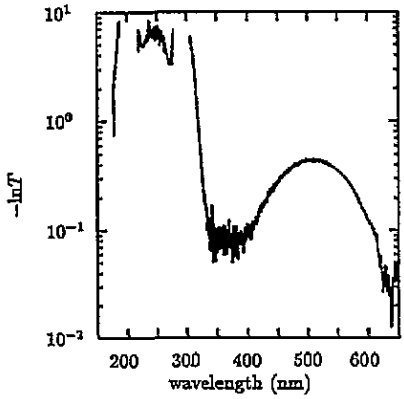

Figure 3. Negative of the natural logarithm of the optical transmission T of a 0.35 mm thick BaF_2:Ce (2.6 mol.%) crystal, after x-irradiation. The wavelength resolution is 8 Å FWHM.

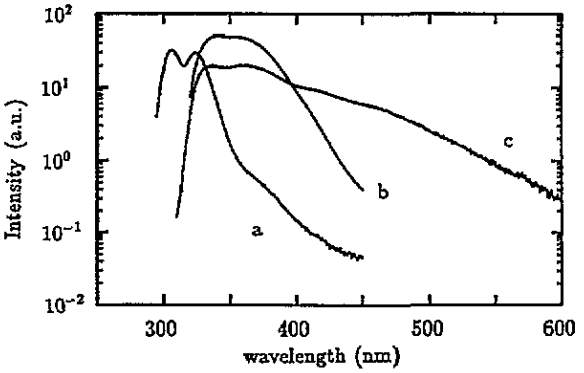

Figure 4. UV-induced emission per incident lamp photon at different wavelengths λ_{exc} of the exciting radiation. The cerium concentrations are (a) 0.0012, (b) and (c) 0.83 mol.%. λ_{exc} = (a) 285, (b) 310, and (c) 245 nm. Shown is the photon output per unit wavelength in arbitrary units. The resolutions are $\Delta\lambda_{exc} = 9$ Å and $\Delta\lambda_{em} = 5$ Å (FWHM).

3.1.2. Emission. Emission spectra, obtained by exciting the crystals with UV photons, are shown in figure 4. It is clear that different emission bands are excited by photons of 290 nm, 310 nm or 245 nm wavelength. We performed excitation measurements to find out which absorption bands are related to each emission band. For this, we chose emission wavelengths λ_{em}, at which the emission bands do not overlap too much with each other. These are 323 nm for the 0.0012 mol.% doped crystal, and 380 nm and 465 nm for the 0.83 mol.% doped crystal. The results are shown in figure 5. The excitation spectra show clear similarities with the absorption spectra in figure 2. The excitation peak at 290 nm in figure 5, curve a, corresponds to the Ce_1 absorption peak. The excitation peak at 310 nm in curve c corresponds to Ce_2 absorption, and the excitation structure near 245 nm in curve d is assigned to Ce_3. Also shown in figure 5 is the excitation spectrum of the 0.0012 mol.% doped crystal at $\lambda_{em} = 380$ nm (curve b). This clearly shows the presence of Ce_2 in this sample, too.

From the above, we can conclude that spectrum a in figure 4 is mainly due to Ce_1 emission, spectrum b to Ce_2 emission, and spectrum c to Ce_3 emission. By subtracting the contributions of Ce_2 and Ce_3 emissions to the spectrum a, we obtained the pure

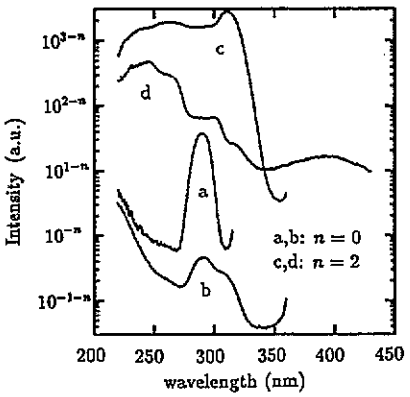

Figure 5. Excitation spectra of BaF_2:Ce. (a) and (b) apply to a 1.85 mm thick 0.0012 mol.% doped sample, (c) and (d) to a 1.9 mm thick 0.83 mol.% doped one. The emission wavelengths λ_{em} (in nm) are (a) 323, (b) 380, (c) 380 and (d) 465. The resolutions $\Delta\lambda_{exc}$, $\Delta\lambda_{em}$ (FWHM, in Å) are (a) 5, 9; (b) and (c) 9, 17; (d) 9, 9.

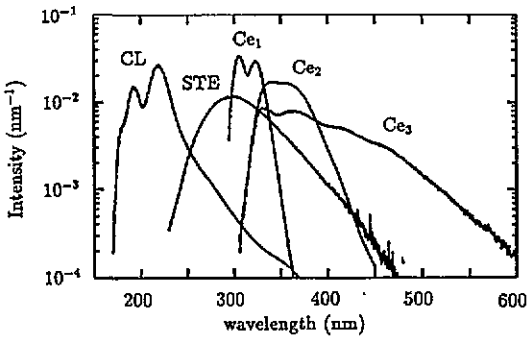

Figure 6. The five bands that were present in the emission spectra. As displayed, the wavelength integral of each band is one. The resolution for the CL and STE bands is 42 Å; for the other bands it is 5 Å FWHM.

Ce_1 emission band. In a similar way the Ce_2 emission band was obtained. The Ce_3 emission is somewhat of a problem. Whereas the Ce_1 and Ce_2 bands both show two peaks, which is due to the spin–orbit splitting of the Ce^{3+} $4f^1$ states, curve c is more complicated. There is clearly a contribution from Ce_1 and Ce_2 in it, but even beside that it is probably due to several different centres. We subtracted only some Ce_2 contribution. The resulting emission bands are shown in figure 6. Also shown are the STE and CL emission bands, which were obtained by exciting the crystal with x-rays. The STE band was also excited using 133 nm photons.

From the emission spectra in figure 4, we determined the relative quantum efficiencies of the crystals. Using the absorption coefficients for 290 nm, 310 nm and 245 nm photons, we calculated the fraction of the incident photons that was absorbed in the crystals. Dividing the wavelength integral of the spectra in figure 4 by this fraction yielded the relative quantum efficiencies. Within an error of about 20%, these were the same. The absolute quantum efficiency was difficult to estimate. In any case it was high. High quantum efficiencies were also reported in Ce^{3+} doped LaB_3O_6 crystals and glasses, and in $LiLaP_4O_{12}$ glass, and no increase of the emission was found on cooling from room temperature down to 4.2 K [28, 29]. Also, in several other crystal hosts, including CaF_2, no thermal quenching of Ce^{3+} luminescence at room temperature was observed [30, 31]. This suggests that the quantum efficiency of Ce^{3+} in BaF_2 is close to 1.

For interpreting the luminescence decay under gamma irradiation, we needed to know the 1/e decay times of the Ce_1, Ce_2 and Ce_3 centres. Therefore, we irradiated some samples with UV photons from the flash lamp. The wavelength λ_{exc} of the radiation was chosen such that either of the three centres was selectively excited. The emission was recorded at wavelengths λ_{em} characteristic of either cerium emission band, as a function of time. The results are shown in figure 7.

The decay curves can be described as $I = I_0 \exp(-t/\tau)$. The decay times τ,

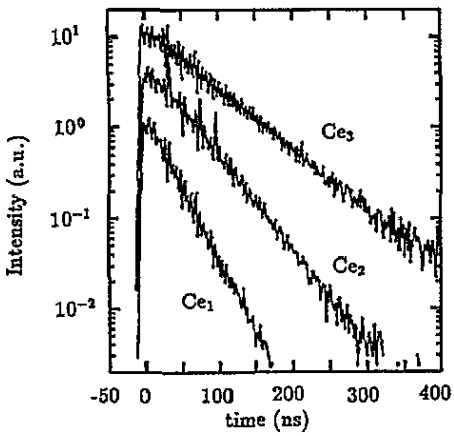

Figure 7. The decay of the luminescence of the centres Ce_i. Ce_1 in BaF_2:Ce (0.0012%), $\lambda_{exc} = 289$ nm and $\lambda_{em} = 323$ nm; Ce_2 in BaF_2:Ce (0.83%), $\lambda_{exc} = 310$ nm and $\lambda_{em} = 370$ nm; Ce_3 in BaF_2:Ce (0.83%), $\lambda_{exc} = 245$ nm and $\lambda_{em} = 470$ nm. The samples are 1.9 mm thick. The time resolution is 6 ns; the wavelength resolutions are 10 nm (FWHM). The contribution of the Ce_i centres, other than indicated, is less than 1% for each curve.

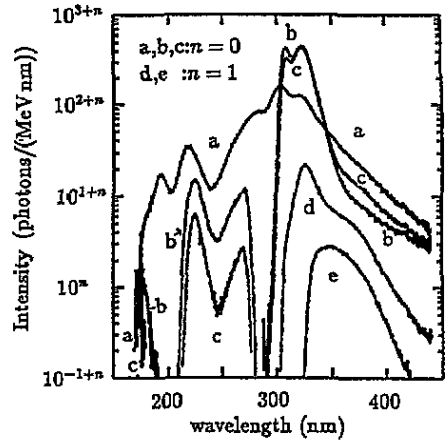

Figure 8. X-ray induced luminescence of several BaF_2:Ce crystals. The cerium concentration (mol.%) is (a) 0.0012, (b) 0.17, (c) 0.38, (d) 0.83 and (e) 4.9. The thickness of the crystals is 1.9 mm. The resolution is 42 Å FWHM.

determined from the curves in figure 7, are 27±3 ns for Ce_1, 42 ± 3 ns for Ce_2, and 65 ± 5 ns for Ce_3. Due to radiative trapping, the experimentally observed decay time may deviate from the intrinsic decay times of the centres. In the appendix we show that this is not the case for the above numbers. These decay times are typical of Ce^{3+} luminescence in a variety of environments. Among these are aqueous solutions [32, 33], and a variety of crystals [13, 30, 31]. The increase of the decay time in the sequence Ce_1–Ce_2–Ce_3 can be related to the ν^3 dependence of the emission rate.

3.2. Luminescence under x- and gamma-ray excitation

Figure 8 shows the emission spectra obtained by irradiating BaF_2:Ce samples with x-rays. The unit 'photons MeV^{-1} nm^{-1}' denotes the number of photons emitted from the crystals per MeV of x-ray energy absorbed in the crystal and per nm wavelength. The calibration is based on a comparison with a sample of pure BaF_2. The photon output of pure BaF_2 was reported to be 1.1×10^4 photons per MeV [34]. The luminescence bands of figure 6 can be recognized in the spectra of figure 8. Note that part of the emission is re-absorbed by the crystal (cf figure 2). Figure 8 shows that at low cerium concentrations, CL, STE and Ce_1 emission bands dominate. The higher the cerium concentration, the lower are the CL and STE emissions. Near 0.83 mol.% cerium concentration, Ce_2 emission appears, and at even higher concentrations it dominates the emission spectrum. The total emission intensity decreases at these higher concentrations.

We are interested in the contribution of each centre to the observed x-ray induced emission spectra. Since exciting x-rays incident on one side of the crystal penetrated it by only about 0.1 mm, luminescence photons must be transmitted through the crystal

before detection of them is possible at the other side. The emission bands shown in figure 6, multiplied by the optical transmission spectra $\exp[-\mu(\lambda)d]$ of the bulk of the crystal, then give the shape of the emission bands emerging from the detection side of the crystal (in the above expression, d is the crystal thickness and $\mu(\lambda)$ is the absorption coefficient; see figure 2). Comparing these bands to the emission spectra of figure 8 provides the contribution of each centre to the x-ray induced emission spectra. This is shown in figure 9 as a function of cerium concentration. Next, we corrected these contributions for the photons 'missed' because of optical absorption in the crystals. This amounts to dividing the observed emission bands by the transmission spectra. This correction provides the 'absorption-corrected' photon outputs shown in figure 10.

The absorption correction is justified only if the absorbed photons from a centre 'A', say, are not re-emitted by another centre of type 'A'. This will be so for the CL and STE centres, because CL and STE emission cannot excite CL and STE centres respectively [23]. The CL and STE photon output curves in figure 10 represent the actual number of photons created by x-rays in the top layer of the crystals. The absorption correction is not justified for the Ce_1, Ce_2 and Ce_3 centres, for which the emission and absorption spectra more-or-less overlap. Depending on the number of absorbed photons re-emitted by the same type of centre, the number of photons actually created is somewhere between the curves shown in figures 9 and 10.

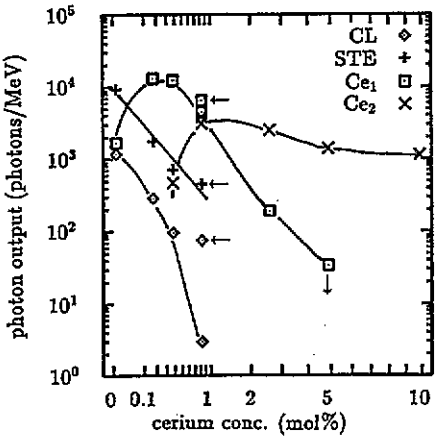

Figure 9. The observed x-ray induced photon outputs due to the CL, STE and Ce_i bands. Most crystals are 1.9 mm thick, except for the 1.6 mm thick 2.6 mol.% and 4.2 mm thick 9.9 mol.% doped ones. The horizontal arrows indicate a 0.38 mm thick sample. Downward pointing arrows mean that the point is an upper limit. The errors in most data points are about the symbol size, but for 0.83 mol.% the error in the STE and the lowest CL data is about a factor 2. Curves are drawn to guide the eye. Note the square root scale of the abscissa.

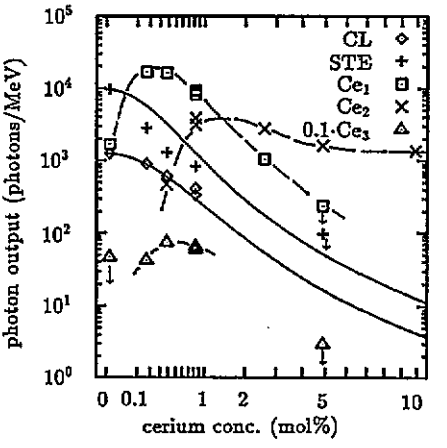

Figure 10. The absorption-corrected x-ray induced photon outputs due to the CL, STE and Ce_i bands. Most crystals are 1.9 mm thick, except for the 1.6 mm thick 2.6 mol.% and 4.2 mm thick 9.9 mol.% doped ones. Half of the data at 0.83 mol.% are due to a 0.38 mm thick sample. Most errors are about the symbol size, but the error in the STE photon output in the 0.83 mol.% doped sample is a factor 2. Downward pointing arrows mean that the point is an upper limit. For the purposes of illustration, the Ce_3 outputs were divided by 10. The full curves represent the calculated STE and CL photon outputs (see text). Note the square root scale of the abscissa.

The luminescence decay was measured using ^{137}Cs gamma quanta with an energy of 662 keV. Different luminescence centres were selected by observing the luminescence decay at several specific wavelengths. The decay curves were calibrated by comparing the time integral of the decay curves to the experimentally observed photon outputs under x-ray excitation (see figures 9 and 10). This procedure may be followed since no emission could be observed at times beyond ~ 1 ms [11].

The decay results are shown in figure 11 for the 0.17 mol.% doped sample. In this figure the decay of CL and STE luminescence recorded at 270 nm wavelength is seen. Moreover, the decay of the Ce_1 luminescence at 323 nm is shown. Figure 12 shows results from the 0.83 mol.% doped sample. Both Ce_1 luminescence, observed at 325 nm, and Ce_2 luminescence at 370 nm are shown. Figure 13 shows the total luminescence from the 2.1 mol.% doped sample, and the luminescence from the 9.9 mol.% doped sample at different wavelengths. The curves in this figure are mainly due to Ce_2 luminescence.

4. Model calculations and discussion

In this section the effects of dipole–dipole and radiative energy transfer on the luminescence are calculated. The equations used for the calculations are presented in subsection 4.1. In subsection 4.2 the experimental photon outputs (figures 9 and 10) are discussed and compared to calculations. In subsection 4.3 the experimental decay curves (figures 11–13) are compared to calculated decay curves.

4.1. Theory

We summarize the equations used in our calculations. They apply to dipole–dipole energy transfer and to radiative energy transfer processes.

In the dipole–dipole interaction, the energy of a donor centre D is transferred to an acceptor centre A at a rate $w_{dd}(r) = (1/\tau_{D,r})(R_0/r)^6$. Here $1/\tau_{D,r}$ is the radiative transition rate of the donor centre and the critical distance R_0 is given by [18]

$$R_0^6 = \frac{3\hbar^4 c^4}{4\pi n^4}\left(\frac{\mathcal{E}}{\sqrt{\kappa}\mathcal{E}_c}\right)^4 \int_0^\infty \mathrm{d}E\, \frac{f_D(E)\,\mu_A(E)}{E^4 N_A} \tag{4.1}$$

where n is the refractive index of the crystal and $\kappa \approx n^2$ is the relative electric permittivity. The term $\mathcal{E}_c$ is the electric field within the crystal and $\mathcal{E}$ that on an atom in a vacuum, such that both fields correspond to the same photon densities. The subscript A denotes the acceptor centre, and D denotes the donor centre. The term N_A is the number density of acceptor centres and $\mu_A(E)$ is their absorption coefficient; $f_D(E)$ is the emission spectrum of the donor centre, normalized in such a way that $\int_0^\infty \mathrm{d}E\, f_D(E) = 1$. Like Dexter, we will approximate $(\mathcal{E}/\sqrt{\kappa}\mathcal{E}_c) = 1$.

Our calculation of dipole–dipole interactions between the centres D and A is based on the following assumptions. (i) The centres are randomly distributed over the lattice; consequently they have no spatial correlation to each other. (ii) They are immobile. (iii) Their concentration is not too high. (iv) The minimal separation between centres D and A is much less than R_0. Assumptions (i)–(iii) seem to be reasonable, at least in lightly doped BaF_2:Ce. Assumption (iv) is true. In BaF_2,

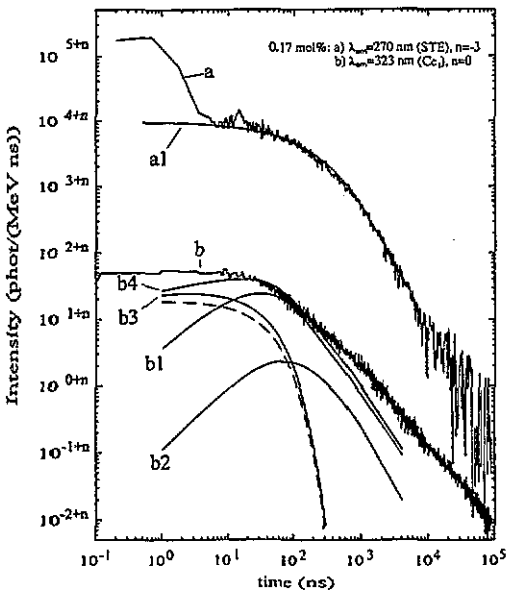

Figure 11. Luminescence decay of 4.3 mm thick BaF_2:Ce (0.17 mol.%). λ_{em} are the emission wavelengths for which the experimental curves were measured (resolution: 16 nm FWHM). For calibration along the ordinate, the x-ray excited photon outputs were used. For this calibration, curve a shows the total absorption-corrected STE emission; curve b shows the total observed Ce_1 emission (not absorption-corrected). Note the different scales of curves a and b, as indicated by the n values. The fitting procedure leading to curve a1 is discussed in the text. The calculated decay curves show STE → Ce_1 transfer by b1 dipole–dipole interaction and b2 photon absorption. Curve b3 is due to both dipole–dipole and radiative CL → Ce_1 transfer; b4 = b1 + b2 + b3. The correspondence of curve b4 to curve b can be improved by adding the broken curve, which represents prompt Ce_1 emission.

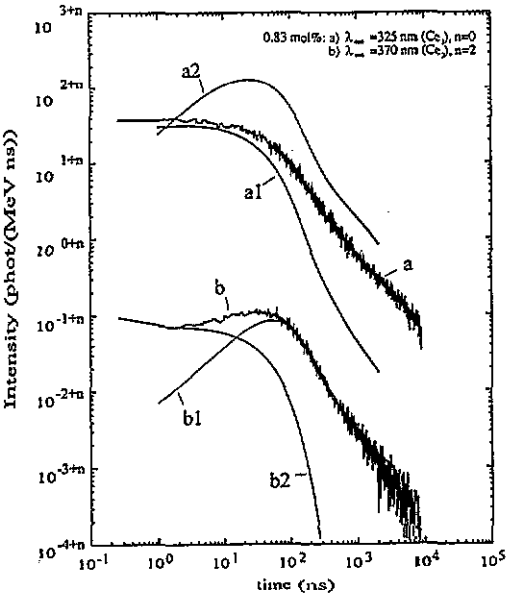

Figure 12. Luminescence decay of 4.4 mm thick BaF_2:Ce (0.83 mol.%). λ_{em} are the emission wavelengths (resolution 16 nm FWHM). Curves a and b are the experimentally observed decay of Ce_1 and Ce_2 centres respectively. X-ray excited photon outputs were used for calibration along the ordinate. For this calibration, curve a shows the total Ce_1 emission after correction for Ce_2 absorption only (this is 1.5 times the not absorption-corrected Ce_1 emission) and curve b shows the observed Ce_2 emission (not absorption-corrected). The calculated curve a1 includes CL → Ce_1 energy transfer (dipole–dipole and radiative) and radiative STE → Ce_1 energy transfer. Curve a2 is calculated for STE → Ce_1 dipole–dipole energy transfer. Curve b1 is curve a convoluted by the Ce_2 decay $\exp(-t/42\,\text{ns})$ and subsequently multiplied by a factor to obtain the best fit. The added exponential b2 represents the decay of promptly excited Ce_2 centres.

the minimum possible separation between D and A centres is typically 3 Å. As we will see later, this is much less than the distances R_0 in the energy transfer processes considered. Under assumptions (i)–(iv), the photon emission rate $L_D(t)$ from centres D may be written

$$L_D(t) = I_D(t) * \frac{1}{\tau_{D,r}} \exp\left(-\frac{t}{\tau_D} - H_D(t)\right) \tag{4.2}$$

where $I_D(t)$ is a function describing the number of D centres excited at time t by whatever means; τ_D is the 1/e decay time of the isolated D centre (i.e. not surrounded by A centres). The decay rate $1/\tau_D$ is the sum of the radiative decay rate, $1/\tau_{D,r}$, and the (thermally activated) non-radiative decay rate, $1/\tau_{D,nr}$. The convolution $*$ is

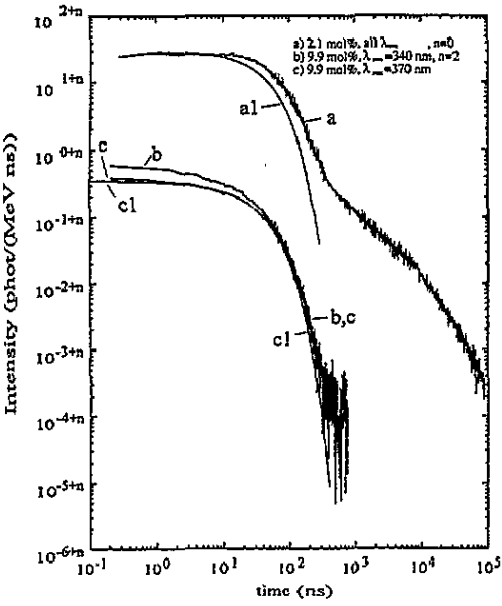

Figure 13. Luminescence decay of 4.3 mm thick BaF_2:Ce of concentrations 2.1 and 9.9 mol.%. λ_{em} are the emission wavelengths (resolution 16 nm FWHM). Curve a is measured without wavelength discrimination. X-ray excited photon outputs were used for calibration along the ordinate. For this calibration, curve a shows the total observed (mainly Ce_2) emission and curve c the Ce_2 emission (both not absorption corrected). Curve b is placed such that the tails of b and c coincide. Curve a1 is $\exp(-t/42\,\text{ns})$ multiplied by an arbitrary constant. Curve c1 is a fit to curve c.

defined by

$$f(t) * g(t) \equiv \int_0^t \mathrm{d}t'\, f(t')\, g(t-t') \tag{4.3}$$

where $t = 0$ is the time at which a gamma is absorbed by the crystal. The second factor in the right-hand side of (4.2) describes the decay of the D centres, once they have been excited. For dipole–dipole energy transfer, we have

$$H_D(t) = \tfrac{4}{3}\pi R_1^3 n_A\, \Gamma(\tfrac{1}{2})\sqrt{t/\tau_D} \qquad R_1 \equiv \left(\frac{\tau_D}{\tau_{D,r}}\right)^{1/6} R_0 \tag{4.4}$$

where n_A is the concentration of A centres. This expression is a generalization of similar expressions holding in the case when no thermal quenching within the D centre is present, i.e. $\tau_D = \tau_{D,r}$ [19,20].

The (time-integrated) photon output from centre D is obtained by integrating (4.2). In the case of a dipole–dipole interaction, (4.4), we obtain

$$\int_0^\infty \mathrm{d}t\, L_D(t) = \left(\int_0^\infty \mathrm{d}t\, I_D(t)\right)\left(\frac{\tau_D}{\tau_{D,r}}\int_0^\infty \mathrm{d}x\, \exp(-x - \tfrac{4}{3}\pi R_1^3 n_A\, \Gamma(\tfrac{1}{2})\sqrt{x})\right). \tag{4.5}$$

In words, the D photon output is the product of the number of D centres excited and a quenching factor. The quenching factor consists of two parts. The first is the factor $\tau_D/\tau_{D,r}$, which accounts for thermal quenching within the D centre. The second is an integral, which we will call the quenching integral. The quenching integral is governed by the quenching parameter $\frac{4}{3}\pi R_1^3 n_A$. The larger this parameter, the smaller the quenching integral (and the light output). We observe that for $\frac{4}{3}\pi R_1^3 n_A \leqslant 0.8$, the quenching integral can be approximated to within 20% accuracy by $\exp(-\frac{\pi}{2}\frac{4}{3}\pi R_1^3 n_A)$.

The photon emission rate from the A centre, excited by D centres through dipole–dipole interaction, is given by

$$L_A(t) = I_D(t) * \frac{dH_D(t)}{dt} \exp\left(-\frac{t}{\tau_D} - H_D(t)\right) * \frac{1}{\tau_{A,r}} \exp\left(-\frac{t}{\tau_A} - H_A(t)\right). \quad (4.6)$$

The middle convolution factor on the right-hand side of (4.6) represents the excitation through the dipole–dipole interaction. For excitation through the absorption of photons from D centres (radiative energy transfer), this factor would be $f_D\,(1/\tau_{D,r})\exp[-t/\tau_D - H_D(t)]$, where the term f_D is the fraction of D photons absorbed by A centres. The last factor on the right-hand side of (4.6) describes the decay of the A luminescence. If this is not quenched by energy transfer to other centres, $H_A(t) = 0$.

The (time-integrated) photon output from centre A is obtained by integrating (4.6). If $H_A(t) = 0$, then we have

$$\int_0^\infty dt\, L_A(t) = \left(\int_0^\infty dt\, I_D(t)\right)\left[1 - \int_0^\infty dt \frac{1}{\tau_D}\exp\left(-\frac{t}{\tau_D} - H_D(t)\right)\right]\frac{\tau_A}{\tau_{A,r}}$$

$$= \left[\left(\int_0^\infty dt\, L_D(t)\right)_{n_A=0} - \left(\int_0^\infty dt\, L_D(t)\right)_{n_A}\right]\frac{\tau_{D,r}\tau_A}{\tau_D\tau_{A,r}}. \quad (4.7)$$

Here, use has been made of (4.2) and the fact that $H_D(t) = 0$ if $n_A = 0$ (cf (4.4)). In words, (4.7) means that the A photon output in a crystal where the A concentration is n_A, is equal to $\tau_{D,r}\tau_A/\tau_D\tau_{A,r}$ times the photon output from the donor centre D in the pure crystal ($n_A = 0$) minus that in the n_A doped crystal. This applies to $D \rightarrow A$ dipole–dipole energy transfer. A similar calculation for radiative energy transfer yields the obvious result

$$\int_0^\infty dt\, L_A(t) = \left(\int_0^\infty dt\, L_D(t)\right)_{n_A} f_D \frac{\tau_A}{\tau_{A,r}} \quad (4.8)$$

i.e. the A photon output is the number of D luminescence photons absorbed by A centres multiplied by the radiative quantum efficiency of the A centre.

4.2. Photon output curves

In this section, we discuss the photon output curves shown in figures 9 and 10. As shown in figure 9, the observed CL and STE photon outputs decrease rapidly on increasing the cerium concentration. This is partly due to CL and STE photon absorption by cerium centres. That this cannot explain all of the decrease is shown by the absorption-corrected CL and STE output curves in figure 10. These curves are still decreasing as a function of concentration. If we assume that this is due to

dipole–dipole energy transfer from CL and STE centres to the main cerium centre, Ce_1 (cf table 1), then we can calculate these curves theoretically as well, using (4.5) with D = CL or STE and A= Ce_1. For this we have to calculate R_1 values. From the experimental absorption (Ce_1: the 200 and 290 nm peaks in figure 2) and emission (figure 6) spectra, we first calculated R_0 using (4.1). Next, R_1 values were calculated according to (4.4). The results are shown in table 2. Knowing the R_1 values, the quenching integral in (4.5) was calculated as a function of the cerium concentration, for D = CL or STE and A = Ce_1 (note that $n_{Ce_1} \approx$ total cerium density). The factor $\int dt\, I_D(t)$, i.e. the number of D centres created, is only known for pure BaF_2. If we assume this to be the same for all cerium doped samples, then we arrive at the theoretical CL and STE photon output curves shown in figure 10.

Table 2. Calculation of the R_1 values for $D \rightarrow A$ dipole–dipole energy transfer. Use was made of (4.1) and (4.4) and experimentally obtained absorption and emission spectra and decay times.

D	A	R_0 (Å)	τ_D (ns)	$\tau_{D,r}$ (ns)	R_1 (Å)
CL	Ce_1	12.5 ± 0.5	0.86 ± 0.04	0.86 ± 0.04†	12.5 ± 0.5
STE	Ce_1	16.4 ± 0.7	630 ± 50	1300 ± 200‡	14.6 ± 0.8
Ce_1	Ce_1	13.2 ± 0.5	27 ± 3§	27 ± 3§	13.2 ± 0.5
Ce_1	Ce_2	19 ± 2	27 ± 3§	27 ± 3§	19 ± 2

† The absence of thermal quenching of CL emission in pure BaF_2 [23, 35] implies that $\tau_{CL,r} = \tau_{CL}$.
‡ Determined from the temperature dependence of STE emission in pure BaF_2 [36].
§ $\tau_D = \tau_{D,r}$: see section 3.1.

These curves may decrease too slowly as a function of cerium concentration if $\int dt\, I_D(t)$ decreases by increasing the cerium concentration, due to competition between cerium centres and CL or STE centres for the available electron–hole pairs. Too slow a decrease also arises if, as well as the Ce_1 centres, other acceptor centres A are important as well. As can be seen, the calculated CL curve fits the data well. This suggests that, up to 1 mol.% concentration, $\int dt\, I_{CL}(t)$ does not depend on the cerium concentration, and that apart from cerium there are no important acceptors of energy from CL centres. On the other hand, the calculated STE curve decays more slowly as a function of cerium concentration than the experimental data. This may indicate that fewer STE are formed if cerium is added, or that cerium centres are not the only important acceptors of STE energy. We will return to this point in the next section.

We now discuss the cerium photon output curves. At low cerium concentrations, Ce_2 and Ce_3 emissions are very weak. This is due to the very low concentrations of these centres, as shown in table 1. The dominant emission is Ce_1, which initially increases with cerium concentration. We note that by (4.7) and (4.8), CL $\rightarrow$ Ce_1 and STE $\rightarrow$ Ce_1 energy transfer can account for a Ce_1 photon output of at most

$$\sum_{D=CL,STE} \left(\int dt\, L_D(t) \right)_{n_A=0} \frac{\tau_{D,r}}{\tau_D} = 2.1 \times 10^4 \quad \text{photons MeV}^{-1}.$$

Here the photon outputs at 0 mol.% of figure 10 and the decay times in table 2 have been used. As is clear from figure 10, the cerium photon output never exceeds the

above value. This is an indication that the cerium luminescence might be entirely due to energy transfer from CL and STE centres. In the next section this will be discussed in detail for the 0.17 and 0.83 mol.% doped samples.

At higher concentrations, the Ce_1 luminescence decreases, which is accompanied by an increase of the Ce_2 output (figure 9 and 10). This is ascribed to $Ce_1 \rightarrow Ce_2$ transfer, either by radiative or by dipole–dipole transfer. It is caused by the overlap of the Ce_1 emission and the Ce_2 absorption bands. At still larger cerium concentrations, the Ce_2 emission also decreases. In fact, the total luminescence intensity monotonically decreases above 0.2 mol.% [11]. In the next section this decrease will be discussed.

4.3. Luminescence decay

We now present our calculations of the decay of cerium luminescence as shown in figures 11–13. In the calculations we used the equations in section 4.1, thus considering only dipole–dipole and radiative energy transfer. We will assume (i) that the number of CL and STE centres created is independent of the cerium concentration, and (ii) that the cerium centres Ce_1 and Ce_2 have radiative quantum efficiency 1. In the previous section we already observed that assumption (i) may be wrong for the STE, but nevertheless we adopt it as a working hypothesis. At least for the $\leqslant 1$ mol.% doped samples, assumption (ii) (which is equivalent to $\tau_D = \tau_{D,r}$ for $D = Ce_1, Ce_2$) is probably correct, as was discussed in section 3.1. Below we consider the results for the 0.17, 0.83, 2.10, and 9.9 mol.% doped samples.

4.3.1. Results for 0.17 mol.%. Figure 11 shows the decay of the STE emission (curve a) and of the Ce_1 emission (curve b) in the 0.17 mol.% doped sample. We fitted the STE emission using (4.2). It turns out that $H_{STE}(t) \neq 0$, indicating the existence of energy transfer from STE centres to other centres (e.g. Ce_1). Using the fitting parameters obtained from curve a we could calculate the Ce_1 emission according to our model and compare this to curve b. Below, we first discuss the fitting of the STE emission. Then the calculation of the Ce_1 emission is presented.

STE. For the fit of the STE decay curve a in figure 11 we use (4.2) and (4.4). Here D = STE and A is any centre to which the STE transfers its energy non-radiatively. In (4.2) no explicit expression for the STE creation function $I_{STE}(t)$ is given. In our model (figure 1), STE are created from e–h pairs at very short times, and from trapped electrons and holes at longer times. Therefore, the function $I_{STE}(t)$ consists of two contributions. The first is approximately a delta function of time, describing instantaneous creation. The second describes creation by recombination of two centres where diffusion plays a role. For this process, we assume $\mathrm{d}/\mathrm{d}t\, n_h = -a\, n_h^2$, where $n_h(t)$ is the concentration of either of the recombining centres. The centres may be trapped hole and electron centres. After solving the equation for the second contribution to $I_{STE}(t)$, we arrive at

$$I_{STE}(t) = n_0\, \delta(t) + \frac{a\,[n_h(0)]^2}{[1 + a n_h(0) t]^2}. \tag{4.9}$$

We found the parameter values $n_0 = (1.3 \pm 0.1) \times 10^4$ quanta per MeV, $n_h(0) = (6 \pm 1) \times 10^3$ quanta per MeV, and $a\, n_h(0) = 8.3 \times 10^{-4 \pm 0.3}\ \mathrm{ns}^{-1}$ by fitting the STE luminescence (see figure 11, curve a1). We will refer to the function $I_{STE}(t)$ of (4.9) with the above parameters as $I_{STE}^{0.17}(t)$.

For the function H_{STE}, we found the quenching parameter value $\frac{4}{3}\pi R_1^3 n_A = 1.0 \pm 0.2$ from the fit. This value of the quenching parameter leads to the following two observations. First, in the 0.17 mol.% doped sample, the (absorption-corrected) STE photon output $\int dt\, L_{STE}(t)$ is 0.29 times that in the 0 mol.% doped sample, which follows from the experimental data in figure 10. By (4.5), this is caused by the number $\int dt\, I_{STE}(t)$ of STE created and/or the quenching integral being smaller *in the 0.17 mol.% doped crystal than in the 0 mol.% doped crystal. The quenching* integral follows from the quenching parameter $\frac{4}{3}\pi R_1^3 n_A$: if this is 1.0 ± 0.2 then the quenching integral is 0.28 ± 0.07. Within errors this equals 0.29, meaning that the number of STE formed in the 0.17 mol.% doped sample does not significantly differ from that in the 0 mol.% doped one. In other words, assumption (i) made at the beginning of this section is confirmed for the 0.17 mol.% doped sample. Second, we can calculate n_A from the quenching parameter 1.0 ± 0.2 using $R_1 = 14.6$ Å (table 2). Generally, such a calculation yields an *effective* concentration of acceptor centres, since for not all acceptor centres does $R_1 = 14.6$ Å necessarily hold. We obtain $n_A = (8 \pm 2) \times 10^{25}\,m^{-3} = 0.46 \pm 0.12$ mol.%, i.e. 2.7 ± 0.7 times larger than the 0.17 mol.% cerium concentration. This suggests that some STE-quenching process other than the STE $\rightarrow$ Ce_1 dipole–dipole energy transfer process exists. That this is not improbable becomes clear if we look at lanthanum-doped BaF_2, which was considered in previous papers [6,36]. Lanthanum does not show absorption bands, which according to our model would mean that STE luminescence is not quenched. But on the contrary, STE quenching is observed in BaF_2:La. A similar process (the nature of which is not clear) could be involved in BaF_2:Ce too, in addition to the ones taken into account by our model.

Ce_1. Figure 11, curve b, shows the decay of the Ce_1 luminescence in this sample. For comparing this to theory, we calculated the Ce_1 luminescence as being due to the following four cases.

(i) CL $\rightarrow$ Ce_1 dipole–dipole energy transfer. For this, (4.6) was used for D = CL and A = Ce_1. $I_{CL}(t) \propto \delta(t)$ was taken because CL centres are only created in the first short period of time when hot free electrons and holes exist. The function $H_D(t)$ (cf (4.4)) is determined by R_1 for D = CL and A = Ce_1, and τ_{CL}, which are given in table 2, and by $n_{Ce_1} = 0.17$ mol.% $= 2.86 \times 10^{25}\,m^{-3}$. The function $(t/\tau_{Ce_1}) + H_{Ce_1}(t)$ is determined by the centres to which Ce_1 can transfer its energy. From the R_1 value for D = Ce_1 and A = Ce_2 (table 2) and the very small concentration of Ce_2 centres in this sample (table 1), it follows that $Ce_1 \rightarrow Ce_2$ energy transfer by dipole–dipole interaction is very small. Indeed, hardly any Ce_2 luminescence was observed. $Ce_1 \rightarrow Ce_1$ dipole–dipole energy transfer is not negligible, but does not affect the decay of the Ce_1 luminescence. Not negligible in the 4.3 mm thick sample is $Ce_1 \rightarrow Ce_1$ radiative energy transfer, i.e. by re-absorption of Ce_1 photons. This effectively augments the Ce_1 decay time (see the appendix). Hence, we put $H_{Ce_1}(t) = 0$ and $\tau_{Ce_1} = 37$ ns (the effective Ce_1 decay time in a relatively thick sample).

The above procedure yields a decay curve, determined up to a proportionality constant. This constant was obtained using (4.7). For the 0 and 0.17 mol.% doped samples, the integrals $\int dt\, L_{CL}(t)$, which are the absorption-corrected CL photon outputs, were obtained from figure 10. The decay times of table 2 were used. In this way the Ce_1 photon output $\int dt\, L_{Ce_1}(t)$ due to the CL $\rightarrow$ Ce_1 dipole–dipole energy transfer process was obtained. This determines the above proportionality constant.

(ii) CL → Ce_1 radiative energy transfer. The calculation is just as that of (i), but now (4.6) with the factor $dH_D(t)/dt$ replaced by $f_D/\tau_{D,r}$, is used. Also, instead of (4.7), equation (4.8) was used. The term f_{CL}, the fraction of CL photons absorbed by Ce_1 centres, was obtained from the CL emission and Ce_1 absorption spectra.

(iii) STE → Ce_1 dipole–dipole energy transfer. For this, (4.6) was used with D = STE and A = Ce_1. The proportionality $I_{STE} \propto I_{STE}^{0.17}(t)$ was taken, which function was discussed above. The function $H_{STE}(t)$ in (4.6) is determined by R_1 for D = STE, A = Ce_1 and by τ_{STE} (see table 2), and further by the concentration n_A of STE luminescence quenching centres. For n_A we used the value 0.46 ± 0.12 mol.%, which was obtained above from the fitting of the STE decay curve. The terms τ_{Ce_1} and $H_{Ce_1}(t)$ are as in (i).

The above determines the decay curve up to a proportionality constant. We could determine this constant from (4.7) for D = STE and A = Ce_1. However, the fit of the STE decay curve suggests that only a fraction $1/(2.7 \pm 0.7)$ of the STE energy transferred is received by Ce_1 centres, because of the presence of STE luminescence quenching centres (acceptors) other than Ce_1. Therefore, we determined the Ce_1 photon output due to STE → Ce_1 dipole–dipole energy transfer from (4.7), but with the right-hand side divided by 2.7.

(iv) STE → Ce_1 radiative energy transfer. The calculation is as in (iii), but with the factor $dH_D(t)/dt$ in (4.6) replaced by $f_D/\tau_{D,r}$. Equation (4.8) was used instead of (4.7).

The sum of the decay curves calculated above (i)–(iv) describes the rate $L_{Ce_1}(t)$ at which photons are emitted from Ce_1 centres. In the 0.17 mol.% sample, some of these photons are absorbed by other Ce_1 centres, but due to assumption (ii) at the beginning of this section they will be re-emitted. Hence, $L_{Ce_1}(t)$ should be compared to the observed, not absorption-corrected, Ce_1 emission. This emission is shown by curve b in figure 11, the time-integral of which equals the Ce_1 photon output for 0.17 mol.% doping concentration in figure 9.

The results of the calculations are shown in figure 11 as well. The time integral of the total calculated curve (b4 in figure 11) is $(7.3 \pm 0.7) \times 10^3$ photons MeV^{-1}, whereas the time integral of the experimental Ce_1 photon output (curve b) is $(1.32 \pm 0.13) \times 10^4$ photons MeV^{-1}. The difference between these two numbers is mainly due to the extra Ce_1 luminescence in curve b at long times. This may be caused by (self-) trapped electron and hole centres. It cannot be excluded that these centres are the STE luminescence quenching centres different from Ce_1. This is because the total number of quanta transferred from CL and STE centres is $(1.63 \pm 0.16) \times 10^4$ photons MeV^{-1}, which can account for all of the observed $(1.32 \pm 0.13) \times 10^4$ photons MeV^{-1} Ce_1 emission. The number $(1.63 \pm 0.16) \times 10^4$ photons MeV^{-1} was calculated using (4.7) and (4.8) for D = CL, STE, without dividing the right-hand side of (4.7) by 2.7.

4.3.2. Results for 0.83 mol.%. We will consider the Ce_1 emission, curve a in figure 12, and the Ce_2 emission, curve b, separately.

Ce_1. The Ce_1 emission due to energy transfer from CL and STE centres was calculated in the same way as discussed for the 0.17 mol.% sample (i)–(iv). We used $n_{Ce_1} = 0.83$ mol.% and $\tau_{Ce_1} = 37$ ns. Because no direct measurements of the STE decay were possible for the 0.83 mol.% doped sample, $I_{STE}(t) \propto I_{STE}^{0.17}(t)$ was assumed. The $\frac{4}{3}\pi R_1^3 n_A$ value for STE → Ce_1 dipole–dipole energy transfer was derived from the fact that the experimental STE photon output for the 0.83 mol.%

sample in figure 10 is $0.086 \times 10^{\pm 0.3}$ times that in the 0% sample. The error in this value is due to the uncertainty in the very small STE photon output in the 0.83 mol.% sample. Since for the 0 mol.% doped crystal the quenching integral in (4.5) is 1, the above means, if $\int \mathrm{d}t\, I_{\mathrm{STE}}(t)$ in the 0.83 and 0 mol.% samples are equal, that the quenching integral for the 0.83 mol.% doped crystal is $0.086 \times 10^{\pm 0.3}$. This means that $\frac{4}{3}\pi R_1^3 n_A = 2.4 \times 10^{\pm 0.2}$.

Using $R_1 = 14.6$ Å (table 2), from this quenching parameter the effective concentration of acceptor centres follows as $n_A = 1.8 \times 10^{26 \pm 0.2}\,\mathrm{m}^{-3} = 1.1 \times 10^{\pm 0.2}$ mol.%. Within errors, this effective concentration equals the Ce_1 concentration of 0.83 mol.%. Therefore, the existence of quenching centres other than cerium centres was neglected. In the calculation of the STE $\rightarrow$ Ce_1 decay curve use was made of (4.7) as it is (without dividing the right-hand side by some factor, as we did for the 0.17 mol.% case).

In the calculation, we did not take $Ce_1 \rightarrow Ce_2$ energy transfer into account. This means that the calculations should be compared to the Ce_2-absorption-corrected Ce_1 luminescence, which is represented by curve a in figure 12. The neglect of non-radiative $Ce_1 \rightarrow Ce_2$ energy transfer is not considered to have much impact on the calculated Ce_1 decay curve: under optical excitation we observed an effective Ce_1 decay time $\tau_{\mathrm{eff}} = 34 \pm 3$ ns, which is not very different from the 37 ± 3 ns observed in the 0.17 mol.% sample (see the appendix).

The results of the calculation are shown in figure 12 (curves a1 and a2). We observe that a large part of the experimental Ce_1 curve is explained by CL $\rightarrow$ Ce_1 transfer and by radiative STE $\rightarrow$ Ce_1 energy transfer. Also we see that the calculated STE $\rightarrow$ Ce_1 dipole–dipole energy transfer component is much too large. This may be due to two reasons. First, $\int \mathrm{d}t\, I_{\mathrm{STE}}(t)$ in the 0.83 mol.% doped sample may be smaller than in the 0 mol.% doped sample (this is against our assumption (i) made at the beginning of the section). This implies that the experimental STE photon output at 0.83 mol.% should lie appreciably lower than the theoretical curve. Due to the large error in the experimental value, this cannot be excluded. Second, non-radiative decay processes are not included in our calculation.

Ce_2. We now turn to curve b in figure 12, i.e. the Ce_2 luminescence. For the 0.83 mol.% doped sample, using tables 1 and 2 we calculate $\frac{4}{3}\pi R_1^3 n_{Ce_2} = 0.034$, for the $Ce_1 \rightarrow Ce_2$ transfer. This means that only 5% of the Ce_1 centres would transfer to Ce_2 (equation (4.5) for D = Ce_1 and A = Ce_2). However, for the $Ce_1 \rightarrow Ce_1$ process we calculate $\frac{4}{3}\pi R_1^3 n_{Ce_1} = 1.34$. This means that a Ce_1 centre has an 80% probability of transferring its energy to another Ce_1 centre, instead of decaying radiatively. The energy migration resulting from this enhances the $Ce_1 \rightarrow Ce_2$ transfer.

Apart from this non-radiative $Ce_1 \rightarrow Ce_2$ transfer, Ce_2 centres will also be excited after absorbing a photon emitted by a Ce_1 centre (radiative transfer). For making an estimate of the relative importance of non-radiative and radiative $Ce_1 \rightarrow Ce_2$ transfer, we compared the Ce_1 and Ce_2 photon outputs, under x-irradiation, for 0.38, 1.88, and 4.4 mm thick BaF_2:Ce(0.83 mol.%) samples. By extrapolation, we found that in a 0 mm thick sample, for which radiative $Ce_1 \rightarrow Ce_2$ transfer is absent, the Ce_1:Ce_2 ratio of the photon outputs is about 0.73:0.27. The photon output of Ce_2 due to direct Ce_2 excitation is expected to be very much smaller than the Ce_1 output, because of the low Ce_2 concentration (see table 1). Almost all of the Ce_2 photon output observed will therefore be due to $Ce_1 \rightarrow Ce_2$ transfer. The above ratio then shows that about 27% of the Ce_1 excitation is transferred non-radiatively to Ce_2.

For the thicker crystals, absorption of Ce_1 photons lowered the observed Ce_1 output and the Ce_2 output was observed to increase. In the 4.4 mm thick sample, which was also used in the luminescence decay measurements, the observed $Ce_1 : Ce_2$ output ratio was about 0.33:0.67. If the Ce_2 centre has a luminescence quantum efficiency of 1, then the sum of the photons emitted by Ce_1 and Ce_2 centres is independent of the thickness of the crystal. The above ratios then show that in the 4.4 mm thick sample, about $(0.67-0.27)/0.67 = 60\%$ of the Ce_2 luminescence is due to radiative $Ce_1 \rightarrow Ce_2$ transfer.

For ease of calculation, we assumed that, instead of 60%, 100% of the $Ce_1 \rightarrow Ce_2$ transfer was radiative. Then the Ce_2 decay curve is proportional to the convolution of the experimental Ce_1 decay, curve a in figure 12, and the exponential Ce_2 decay function $\exp(-t/\tau_{Ce_2})$. Choosing the proportionality constant for the best fit to the experimental Ce_2 curve b results in curve b1 in figure 12. This curve accounts for 80% of curve b. As for the 0.17 mol.% sample, the fit can be improved by adding a prompt decay component (curve b2) to curve b1. In the Ce_1 luminescence, curve a, such a prompt component may also be present.

4.3.3. Results for 2.10 mol.%. Due to the relatively high Ce_2 concentration in the 2.10 mol.% doped sample, energy transfer is fast. Therefore, we expect that the decay differs not too much from the intrinsic Ce_2 decay behaviour $\propto \exp(-t/42\,\text{ns})$. As shown in figure 13, curves a and a1, this is indeed the case.

4.3.4. Results for 9.9 mol.%. Also shown in figure 13 is the decay of the (mainly Ce_2) luminescence in the 4.2 mm thick BaF_2:Ce (9.9 mol.%) crystal (curves b and c). Energy transfer is very fast in this sample, and can be considered as instantaneous. A reasonable fit to the decay measured at 370 nm is described by the expression for dipole quenched luminescence, $\exp[-t/\tau - H(t)]$, with the Ce_2 decay time $\tau = 42$ ns. The term $H(t)$ is as in (4.2), with $\frac{4}{3}\pi R_1^3 n_A = 0.2$ obtained from fitting. The fit is shown by curve c1 in figure 13. At 340 nm we observe a slightly steeper decay curve in the short-time regime. A similar effect was also observed by Anderson in pure CeF_3 [37]. This may be due to the presence of Ce_1 luminescence at 340 nm, which is absent at 370 nm (cf figure 6). Note that the data of figure 10 do not exclude the existence of some Ce_1 luminescence at 9.9 mol.%. This luminescence decays very quickly due to the $Ce_1 \rightarrow Ce_2$ dipole–dipole energy transfer, which would explain the steeper luminescence decay observed at 340 nm. We note that Ce_3 luminescence cannot explain the differences in steepness of the decay as a function of wavelength. The contribution of Ce_3 emission (see figure 6) to the luminescence between 340–370 nm, as estimated from the BaF_2:Ce (9.9 mol.%) emission spectrum under x-irradiation, is less than about 2%. If the effect were due to Ce_3, this contribution should be at least 10%.

5. Conclusions

In this paper, we have shown that the emission from BaF_2:Ce under high-energy photon irradiation is composed of five different emission bands. The CL and STE emission bands are due to the host crystal. The other three emission bands are dopant related. These bands, Ce_1, Ce_2 and Ce_3, are centred at about 320, 350 and

380 nm and their intrinsic decay times are 27, 42 and 65 ns respectively. The nature of these bands was discussed.

Under x-irradiation, for <1 mol.% doped crystals, the main cerium emission is due to Ce_1. Above 1 mol.%, Ce_2 is dominant in our samples. By doping, the CL and STE emission bands are strongly reduced. These observations were explained by CL $\rightarrow$ Ce_1 and STE $\rightarrow$ Ce_1 energy transfer, dipole–dipole transfer being the dominant process. At the higher cerium concentrations, $Ce_1 \rightarrow Ce_2$ transfer becomes important.

From a comparison of the photon outputs and the decay curves observed to model calculations, we arrive at the following interpretation of the luminescence in BaF_2:Ce.

First, it is possible that almost all cerium luminescence is due to energy transfer from CL and STE centres. But in the first few nanoseconds, the observed cerium luminescence is too intense for this. This is ascribed to excitation of cerium by hot electrons and holes.

Second, no indication was found of a decrease of the number of created CL centres as the cerium concentration is increased. These CL centres directly transfer their energy to the cerium centres, the energy transfer being faster and more complete at higher cerium concentrations.

Third, the STE centres transfer their energy not only to cerium centres, but also to other centres. It can not be excluded that these other centres eventually excite the cerium centres.

Fourth, at the higher cerium concentrations, the photon output decreases. This is ascribed to a decrease in the number of STE created and/or luminescence quenching processes not included in our model.

For use of the crystal in a scintillation detector with timing capabilities, one desires a high light-yield, combined with fast luminescence decay. For BaF_2:Ce, the former means that a concentration of about 0.2 mol.% should be chosen. However, at this concentration the decay is slowest. Therefore, a higher concentration may be favourable. But beyond 1 mol.%, the emission decreases rather quickly as a function of concentration. As a compromise, one might choose 1 mol.%. If our interpretation of the Ce_2 centre, as being a $Ce^{3+}-O^{2-}$ centre, is correct, then such 1 mol.% doped crystals should be grown oxygen-free. Otherwise, the Ce_2 will dominate the luminescence and slow down the decay.

Acknowledgments

These investigations in the program of the Foundation for Fundamental Research on Matter (FOM) were supported by the Netherlands Technology Foundation (STW).

Appendix

If one observes exponential decay of luminescence, the corresponding decay time is not always the decay time of the centre responsible for the emission. This is illustrated by a measurement of the Ce_1 decay time in a 1.9 mm thick BaF_2:Ce (0.17 mol.%) sample. The experimental conditions were the same as for the Ce_1 decay in figure 7, curve a. However, the observed Ce_1 decay time was not 27 ± 3 ns, but 37 ± 3 ns. After powdering part of the sample, up to a grain diameter of about 30 μm, the observed Ce_1 decay time was 30 ± 3 ns, i.e. equal to the value found for the 0.0012 mol.% doped sample, within errors.

The above is ascribed to re-absorption of Ce_1 photons by other Ce_1 centres in the crystal. This is possible due to the overlap of the Ce_1 emission and absorption spectra. By absorbing the photons, the Ce_1 centres are excited and can decay later. This leads to enhancement of the effective decay time, i.e. the decay time of the observed luminescence. These processes were discussed by Sakai [38], with emphasis on the luminescence from rhodamine B. The formulation used by Sakai was rather general. Below we give a compressed argument, focusing on the case of Ce_1 luminescence.

After excitation of a BaF_2:Ce crystal with an exciting pulse at time $t = 0$, a fraction a_0 of the Ce_1 luminescence is absorbed by Ce_1 centres before reaching the crystal surface. The other fraction, $1 - a_0$, emerges from the crystal. If the total amount of initial Ce_1 luminescence decays as $\exp(-t/\tau)$, then the light directly emerging from the crystal is given by $(1 - a_0)\exp(-t/\tau)$. The absorbed Ce_1 light creates excited Ce_1 centres. The luminescence from these centres is given by

$$a_0\,\eta(e^{-t/\tau}) * \left(\frac{1}{\tau}e^{-t/\tau}\right) = a_0\,\eta(t/\tau)\,e^{-t/\tau} \tag{A1}$$

where η is the probability that an absorbed photon is re-emitted as Ce_1 luminescence. The convolution $*$ is defined by (4.3). Of this secondary light, a fraction a_1 will be absorbed by Ce_1 centres in the crystal, and the fraction escaping the crystal is described by $(1 - a_1)a_0\eta(t/\tau)\exp(-t/\tau)$. The absorbed fraction a_1 yields Ce_1 luminescence described by

$$a_1a_0\,\eta^2(e^{-t/\tau}) * \left(\frac{1}{\tau}e^{-t/\tau}\right) * \left(\frac{1}{\tau}e^{-t/\tau}\right) = \tfrac{1}{2}a_1a_0\,\eta^2\,(t/\tau)^2\,e^{-t/\tau} \tag{A2}$$

of which a fraction $(1 - a_2)$ leaves the crystal, etc. Hence the total amount of Ce_1 light leaving the crystal is

$$\left[(1-a_0) + \sum_{n=1}^{\infty}(1-a_n)\prod_{m=0}^{n-1}a_m\frac{1}{n!}\left(\frac{\eta t}{\tau}\right)^n\right]e^{-t/\tau}. \tag{A3}$$

For not too lightly doped BaF_2:Ce samples, (A3) can be simplified. For these samples, in the wavelength region (290 nm, 365 nm) where the Ce_1 centres emit, the optical transmission is a sharp function of the wavelength. It is either practically zero or almost one for most wavelengths $\in$ (290 nm, 365 nm). Then all a_n in expression (A3) are practically the same, $a_n = a$ say, and (A3) becomes a simple exponential $(1 - a)\exp(-t/\tau_{\text{eff}})$. The effective decay time is $\tau_{\text{eff}} = \tau/(1 - a\eta)$.

Using the above approximate relation for τ_{eff}, an estimate can be made of the importance of the radiative trapping effect for the curves in figure 7. For the BaF_2:Ce (0.0012 mol.%) sample, we calculate that the fraction of the Ce_1 emission re-absorbed over 1.9 mm is $a = 5 \times 10^{-3}$. Hence, τ_{eff} hardly differs from the intrinsic decay time τ. For the Ce_2 and Ce_3 centres the same argument as given above for Ce_1, holds. The fraction of Ce_2 emission, re-absorbed by a 1.9 mm thick BaF_2:Ce (0.83 mol.%) is calculated as $a = 3 \times 10^{-3}$. The fraction of Ce_3 emission re-absorbed by Ce_3 is $a = 0.01$ in this case. Both fractions are very small. We conclude that the observed decay times of figure 7 equal the intrinsic decay times of the respective cerium centres.

We note that the equation $\tau_{\text{eff}} = \tau/(1-a\eta)$ can explain the decay times τ_{eff} from the 0.17 mol.% doped crystals, discussed at the beginning of this appendix. For the

1.9 mm thick sample, the fraction of re-absorbed Ce_1 photons is $a = 0.22$. Since the luminescence efficiency, η, is about one and $\tau = 27 \pm 3$ ns, we calculate $\tau_{eff} = 35 \pm 4$ ns, which is within errors of the experimentally observed value, 37 ± 3 ns. Concerning the powdered sample, the absorbed fraction of Ce_1 photons over a distance of 30 μm is $a \approx 0.01$. This means that the decay time of the Ce_1 luminescence from the powder should equal the intrinsic Ce_1 decay time, which is indeed observed.

References

[1] Ershov N N, Zakharov N G and Rodnyi P A 1982 *Opt. Spektrosk.* **53** 89
[2] Laval M, Moszynski M, Allemand R, Cormoreche E, Guinet P, Odru R and Vacher J 1983 *Nucl. Instrum. Methods* **206** 169
[3] Aleksandrov Yu M, Makhov V N, Rodnyi P A, Syreishchikova T I and Yakimenko M N 1984 *Fiz. Tverd. Tela* **26** 2865
[4] Valbis Y A, Rachko Z A and Yansons Y A 1985 *Sov. Phys.-JETP Lett.* **42** 172
[5] Kubota S, Suzuki M, Ruan J, Shiraishi F and Takami Y 1986 *Nucl. Instrum. Methods* A **202** 291
[6] Visser R, Dorenbos P and van Eijk C W E 1992 *J. Phys.: Condens. Matter* **4** 8801
[7] Czirr J B and Catalano E 1977 *Nucl. Instrum. Methods* **143** 487
[8] Tailor R C, Nestor O H and Utts B 1986 *IEEE Trans. Nucl. Sci.* **NS-33** 243
[9] Rustamov Ya, Tavshunskii G A, Khabibullaev P K, Bessonova T S and Sobolev B P 1987 *Zh. Prikl. Spektr.* **47** 742
[10] Melcher C L, Manente R A and Schweitzer J S 1989 *IEEE Trans. Nucl. Sci.* **NS-36** 1188
[11] Dorenbos P, Visser R, van Eijk C W E, Hollander R W and den Hartog H W 1991 *Nucl. Instrum. Methods* A **310** 236
[12] Visser R, Dorenbos P, van Eijk C W E, Hollander R W and Schotanus P 1991 *IEEE Trans. Nucl. Sci.* **38** 178
[13] Hoshina T 1980 *J. Phys. Soc. Japan* **48** 1261
[14] Visser R, Dorenbos P, Andriessen J and van Eijk C W E 1993 *Nucl. Tracks Radiat. Meas.* in press
[15] Williams R T and Song K S 1990 *J. Phys. Chem. Solids* **51** 679
[16] Andriessen J, Dorenbos P and van Eijk C W E 1991 *Mol. Phys.* **74** 535
[17] Beaumont J H 1970 *Proc. R. Soc.* **315** 69
[18] Dexter D L 1953 *J. Chem. Phys.* **21** 836
[19] Förster Th 1949 *Z. Naturf.* A **4** 321
[20] Galanin H D 1951 *Zh. Eksp. Teor. Fiz.* **21** 126
[21] Bollinger L M and Thomas G E 1961 *Rev. Sci. Instrum.* **32** 1044
[22] Loh E 1967 *Phys. Rev.* **154** 270
[23] Shi C, Kloiber T and Zimmerer G 1988 *J. Luminesc.* **40–41** 189
[24] Manthey W J 1973 *Phys. Rev.* **8** 4086
[25] Andeen C G, Fontanella J J, Wintersgill M C, Welcher P J, Kimble R J Jr and Matthews G E Jr 1981 *J. Phys. C: Solid State Phys.* **14** 3557
[26] Corish J, Catlow C R A, Jacobs P W M and Ong S H 1982 *Phys. Rev.* B **25** 6425
[27] Vakhidov Sh A, Kaipov B, Tavshunskii G A and Gapparov N 1976 *Opt. Spektrosk.* **40** 1099
[28] Verwey J W M and Blasse G 1990 *Mat. Chem. Phys.* **25** 91
[29] Verwey J W M and Blasse G 1990 *Chem. Mater.* **2** 458
[30] Weber M J 1973 *Solid State Commun.* **12** 741
[31] Lyu L-J and Hamilton D S 1991 *J. Luminesc.* **48–49** 251
[32] Kaizu Y, Miyakawa K, Okada K, Kobayashi H, Sumitani M, Yoshihara K 1985 *J. Am. Chem. Soc.* **107** 2622
[33] Okada K, Kaizu Y, Kobayashi H, Tanaka K and Marumo F 1985 *Mol. Phys.* **54** 1293
[34] Dorenbos P, de Haas J T M, Visser R, van Eijk C W E and Hollander R W 1993 *IEEE Trans. Nucl. Sci.* to be published
[35] Schotanus P, van Eijk C W E, Hollander R W and Pijpelink J 1985 *Nucl. Instrum. Methods* A **238** 564
[36] Dorenbos P, Visser R, Dool R, Andriessen J and van Eijk C W E 1992 *J. Phys.: Condens. Matter* **4** 5281
[37] Anderson D F 1990 *Nucl. Instrum. Methods* A **287** 606
[38] Sakai Y, Kawahigashi M, Minami T, Inoue T and Hirayama S 1989 *J. Luminesc.* **42** 317